

LLM-Bootstrapped Targeted Finding Guidance for Factual MLLM-based Medical Report Generation

Cunyuan Yang¹, Dejuan Song², Xiaotao Pang³, Qianqian Shen¹, Wenjie Nie¹,
Yifan Huang¹, Lei Wu¹, Wei Han², Haishuai Wang¹, and Jiajun Bu¹

¹ Zhejiang University

² The Second Affiliated Hospital Zhejiang University School of Medicine

³ Hangzhou Pu Jian Medical Technology Co., Ltd.

Abstract. The automatic generation of medical reports utilizing Multimodal Large Language Models (MLLMs) frequently encounters challenges related to factual instability, which may manifest as the omission of findings or the incorporation of inaccurate information, thereby constraining their applicability in clinical settings. Current methodologies typically produce reports based directly on image features, which inherently lack a definitive factual basis. In response to this limitation, we introduce Fact-Flow, an innovative framework that separates the process of visual fact identification from the generation of reports. This is achieved by initially predicting clinical findings from the image, which subsequently directs the MLLM to produce a report that is factually precise. A pivotal advancement of our approach is a pipeline that leverages a Large Language Model (LLM) to autonomously create a dataset of labeled medical findings, effectively eliminating the need for expensive manual annotation. Extensive experimental evaluations conducted on two disease-focused medical datasets validate the efficacy of our method, demonstrating a significant enhancement in factual accuracy compared to state-of-the-art models, while concurrently preserving high standards of text quality.

Keywords: Medical Report Generation · MLLMs

1 Introduction

The automated generation of medical reports from diagnostic images is a critical task in computational medicine. Early approaches to Medical Report Generation (MRG) relied on encoder-decoder architectures, evolving from CNN-RNN combinations [8, 25, 27] to Transformer-based models [5, 4, 18, 12]. However, they struggled with capturing complex semantic relationships and generating factually precise narratives [16].

The recent advent of Multimodal Large Language Models (MLLMs) [13] has introduced a new paradigm for MRG. MLLMs such as LLaVA-Med [10] have

demonstrated immense potential, yet a significant challenge emerges when fine-tuned end-to-end: factual instability. These models are prone to hallucinating findings or omitting critical pathological observations, which are clinically unacceptable and remain the primary barrier to real-world deployment [3, 26, 24].

Inspired by previous work [9, 23], we hypothesize that this unreliability stems from coupling two distinct cognitive processes in a single model: visual feature recognition and medical language organization. We propose that by decoupling these tasks—first compelling the model to identify all salient clinical facts before composing the report—we can significantly enhance factual accuracy.

A primary obstacle is the lack of large-scale datasets pairing medical images with exhaustive key-finding labels. This is especially pronounced in disease-focused settings, where relevant categories are prohibitively expensive to annotate manually. Prior label-guided methods such as TieNet [25] assume a fixed vocabulary tightly coupled to specific datasets, limiting adaptability and rendering them incompatible with modern MLLM architectures.

To overcome this, we introduce Fact-Flow, a novel framework that improves the factual accuracy of MLLM-based report generation through multi-label guidance. The main contributions are as follows.

- We propose Fact-Flow, which improves MLLM-based report generation via explicit multi-label clinical finding conditioning.
- We design a fully automated, LLM-bootstrapped data pipeline that constructs a large-scale (image, multi-label) dataset from existing image-report pairs without manual annotation.
- We validate Fact-Flow on two disease-focused datasets (ophthalmology and tuberculosis), demonstrating consistent improvements over state-of-the-art methods in NLG metrics and, where applicable, clinical efficacy.

2 Method

We present **Fact-Flow**, a framework that enhances MLLM-based medical report generation through multi-label guidance. Given a training set of medical image-report pairs $\{(I_i, R_i)\}_{i=1}^N$, our goal is to generate a diagnostic report \hat{R} for a new image I that accurately captures all clinical findings. Rather than mapping $I \rightarrow R$ end-to-end, Fact-Flow introduces an intermediate multi-label representation $Y = \{y_1, \dots, y_k\} \in \{0, 1\}^k$, where each y_j denotes the presence or absence of a specific clinical finding. As illustrated in Figure 1, the framework comprises three stages: (1) LLM-bootstrapped label dataset construction, (2) multi-label classification model training, and (3) label-guided report generation, with the predicted labels serving as factual grounding to reduce hallucinations and improve finding recall.

2.1 Stage 1: LLM-Bootstrapped Multi-Label Dataset Construction

Since manually annotating large-scale reports with fine-grained clinical labels is prohibitively expensive, we construct the label dataset automatically via an

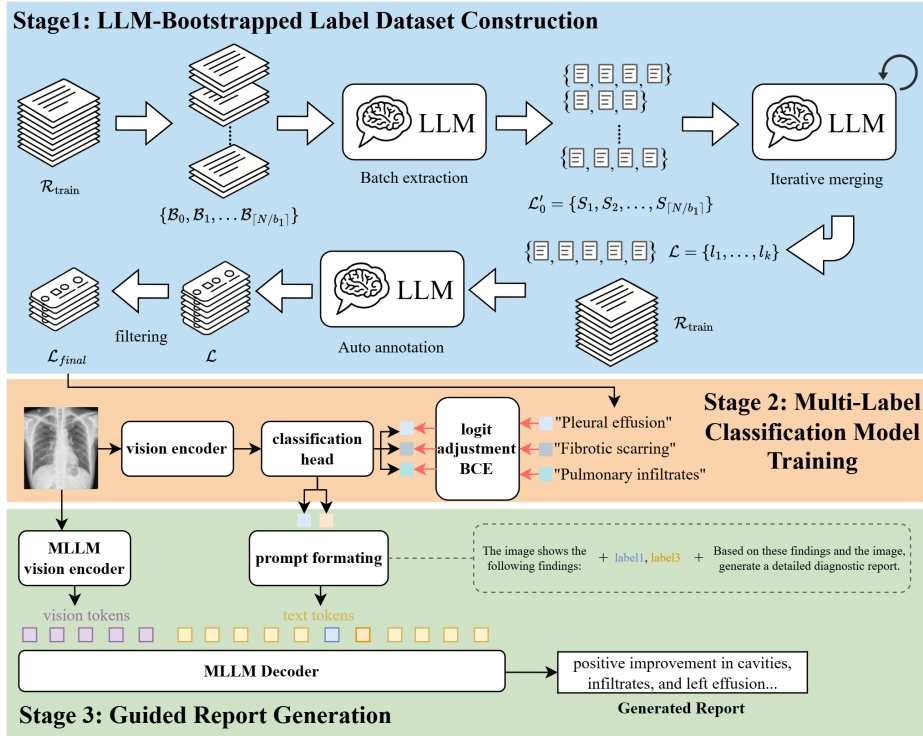


Fig. 1. The overall framework of Fact-Flow

LLM-driven pipeline (see Stage 1 in Figure 1). The pipeline proceeds in two steps.

Taxonomy extraction. We first build a unified label taxonomy $\mathcal{L} = \{l_1, \dots, l_k\}$ from the training reports. Processing all reports in a single LLM call is infeasible due to context-length constraints, so we partition $\{R_i\}_{i=1}^N$ into batches of size b and prompt the LLM to extract clinically significant concepts—including diseases, pathological features, anatomical locations, and severity descriptors—from each batch independently. The resulting per-batch label sets inevitably contain synonyms and redundancies, so we consolidate them through iterative hierarchical merging: at each round, sets are grouped within a token budget κ and the LLM is prompted to perform synonym normalization and deduplication, repeating until a single canonical taxonomy \mathcal{L} is obtained.

Report annotation and filtering. Given \mathcal{L} , we annotate each training report R_i by prompting the LLM to identify all labels explicitly or implicitly mentioned, producing a binary vector $Y_i \in \{0, 1\}^k$ where $Y_i[j] = 1$ if label l_j is present. To reduce annotation noise and mitigate long-tail issues, we apply frequency-based filtering and retain only labels that appear in at least θ reports. This yields the final bootstrapped dataset $\mathcal{D}_{\text{MLC}} = \{(I_i, Y_i)\}_{i=1}^N$ used to train the guidance model in Stage 2.

2.2 Stage 2: Guidance Model Training

In this stage (see Stage 2 in Figure 1), we train a multi-label classification model f_{MLC} , formally defined as $f_{\text{MLC}}(I) = \sigma(W_{\text{cls}} \cdot \phi(I))$, to predict clinical findings from medical images, where $\phi(\cdot)$ is a pre-trained vision encoder (DINOv3 [21] with a ConvNeXt backbone [14]) and $\sigma(\cdot)$ denotes the sigmoid function applied independently per label.

Medical datasets exhibit severe class imbalance, with rare but critical findings appearing in fewer than 1% of cases. Standard binary cross-entropy tends to overlook these tail classes. To address this, we adapt the logit adjustment method [15] to multi-label binary classification, shifting each raw logit z_j by the log-odds of its empirical frequency p_j before computing the loss:

$$\tilde{z}_j = z_j + \tau \log \frac{p_j}{1-p_j} \quad (1)$$

where $p_j = \frac{1}{N} \sum_{i=1}^N Y_i[j]$ is the empirical label frequency and τ is a temperature parameter (set to 1). The adjusted logits \tilde{z}_j are then used in the standard binary cross-entropy loss, re-balancing the decision boundary to improve both precision and recall on tail labels.

2.3 Stage 3: Guided Report Generation

In the final stage (see Stage 3 in Figure 1), we fine-tune a multimodal large language model (MLLM) to generate diagnostic reports conditioned on both visual features and predicted clinical findings.

During training, the bootstrapped ground-truth labels Y_i are serialized into a natural-language prompt (e.g., *“The image shows the following findings: [label_a], [label_b], [label_c]. Based on these findings and the image, generate a detailed diagnostic report.”*), which is prepended to the generation target. The model is optimized with the standard next-token prediction objective, learning to condition its output on both the visual input and the explicit label guidance.

At inference time, the ground-truth labels are unavailable. Instead, the predicted labels $\hat{Y} = f_{\text{MLC}}(I)$ from Stage 2 are serialized into the same prompt format and used to guide generation, grounding the report in explicitly identified factual findings.

3 Experiments

3.1 Dataset and Evaluation Metrics

We evaluate Fact-Flow on two medical imaging datasets. The first is the publicly available tuberculosis chest X-ray dataset [7], comprising 561/80/160 frontal chest X-rays for training, validation, and testing, each paired with a diagnostic report describing tuberculosis-related findings. The second is a multimodal ophthalmology dataset collected from a clinical institution, consisting of 1,854/206/515 cases for training, validation, and testing, with IRB approval for research use.

Each case provides three imaging modalities—fundus photography, Optical Coherence Tomography (OCT), and Optical Coherence Tomography Angiography (OCTA)—paired with a detailed Chinese-language diagnostic report authored by ophthalmologists describing myopia-related complications and retinal changes.

We assess report quality using two sets of metrics. For natural language generation (NLG), we employ BLEU-1 through BLEU-4 [19], ROUGE-L [11], CIDEr [22], and METEOR [2]. For clinical efficacy on the tuberculosis dataset, we adopt RadFact [3], which leverages large language models to extract clinical entities from both generated and reference reports and computes Precision, Recall, and F1-score without requiring predefined disease-specific categories. No established clinical efficacy metric is currently available for Chinese ophthalmology reports, so only NLG metrics are reported for that dataset.

3.2 Implementation Details

For Stage 1 label bootstrapping, we use GPT-5-mini to extract and merge clinical findings from training reports with $b = 200$, $\kappa = 200$, and a merging threshold $\theta = 15$, yielding 7 labels for tuberculosis and 42 for ophthalmology datasets. For Stage 2, the multi-label classifier f_{MLC} employs DINOv3-ConvNeXt-Base [21, 14] as the visual encoder with full fine-tuning and logit adjustment [15] ($\tau = 1.0$) for long-tail optimization, trained with a learning rate of 2×10^{-5} . For the ophthalmology dataset, we use separate encoders for each modality (fundus, OCT, OCTA) with feature fusion. For Stage 3, we fine-tune three MLLMs—Qwen2.5-VL 7B [1], MedGemma 4B [20], and LLaVA-Med-v1.5-Mistral 7B [10]—using LoRA [6] on the decoder, vision encoder, and projector; all models are trained with the AdamW optimizer (learning rate 2×10^{-4} , weight decay 0.1) using BFloat16 mixed precision on four NVIDIA RTX A6000 GPUs.

3.3 Comparison with State-of-the-Art Methods

We compare Fact-Flow against traditional MRG models (R2Gen [5], R2GenCMN [4], R2GPT [26], R2GenCSR [24], CvT2DistilGPT2 [17]), MLLM baselines (Qwen2.5-VL, MedGemma, LLaVA-Med fine-tuned directly on image-report pairs without factual guidance), and powerful closed-source VLMs (Gemini-2.5-Flash and Gemini-2.5-Pro) evaluated in a zero-shot setting. On the tuberculosis dataset (Table 1), our approach consistently improves all three MLLMs across NLG and clinical efficacy metrics. **MedGemma + Fact-Flow** achieves the best overall performance, while vanilla MLLM baselines suffer from mode collapse—Qwen2.5-VL yields perfect precision but near-zero recall, and LLaVA-Med produces zero clinical efficacy scores—a problem our factual guidance directly addresses. Despite their strong general capabilities, Gemini-2.5-Flash and Gemini-2.5-Pro perform poorly in the zero-shot setting, underscoring the necessity of domain-specific training for medical report generation. On the ophthalmology dataset (Table 2), **Qwen2.5-VL + Fact-Flow** achieves the best results on most NLG metrics, demonstrating the effectiveness of our approach across complex multimodal scenarios. Qualitative examples in Table 3 further confirm that factual

Table 1. Comparison with state-of-the-art methods on the Tuberculosis dataset. “+FF” denotes our Fact-Flow approach.

| Type | Method | Clinical Efficacy | | | Natural Language Generation | | | |
|--------------------|------------------|-------------------|---------------|---------------|-----------------------------|---------------|---------------|---------------|
| | | F1 | Prec. | Recall | B-4 | R-L | CIDEr | METEOR |
| <i>Traditional</i> | R2Gen | 0.1909 | 0.2273 | 0.1646 | 0.0682 | 0.6423 | 1.7061 | 0.2131 |
| | R2GPT | 0.2105 | 0.1310 | <u>0.5361</u> | 0.1032 | 0.3101 | 1.1659 | 0.1813 |
| | CvT2DistilGPT2 | 0.2128 | 0.2333 | 0.1957 | 0.1655 | 0.5752 | 1.7217 | 0.1896 |
| | R2GenCSR | 0.2041 | <u>0.3000</u> | 0.1546 | 0.1478 | 0.6333 | 1.8396 | 0.1953 |
| | R2GenCMN | 0.2334 | 0.2903 | 0.1952 | 0.0603 | <u>0.6500</u> | 1.7216 | 0.1990 |
| <i>MLLM</i> | MedGemma | 0.2266 | 0.2422 | 0.2130 | 0.0795 | 0.6566 | 1.7307 | 0.1759 |
| | LLaVA-Med | 0.0000 | 0.0000 | 0.0000 | 0.0242 | 0.4691 | 1.1719 | 0.1177 |
| | Qwen2.5-VL | 0.0286 | 1.0000 | 0.0145 | 0.0265 | 0.4779 | 1.2035 | 0.1141 |
| <i>Zero-Shot</i> | Gemini-2.5-Flash | 0.0677 | 0.0525 | 0.0952 | 0.0014 | 0.0383 | 0.0102 | 0.0295 |
| | Gemini-2.5-Pro | 0.0713 | 0.0457 | 0.1621 | 0.0008 | 0.0301 | 0.0003 | 0.0245 |
| <i>Fact-Flow</i> | MedGemma + FF | 0.3055 | 0.3070 | 0.3041 | 0.2290 | 0.6243 | 2.0664 | 0.2305 |
| | LLaVA-Med + FF | 0.2016 | 0.1974 | 0.2059 | 0.1287 | 0.6018 | 1.5869 | 0.1869 |
| | Qwen2.5-VL + FF | <u>0.2831</u> | 0.3535 | 0.2361 | <u>0.2129</u> | 0.6107 | <u>1.9434</u> | <u>0.2236</u> |

Table 2. Comparison with state-of-the-art methods on the Ophthalmology dataset. “+FF” denotes our Fact-Flow approach.

| Method | BLEU-1 | BLEU-2 | BLEU-3 | BLEU-4 | ROUGE-L | CIDEr |
|----------------------------|---------------|---------------|---------------|---------------|---------------|---------------|
| <i>Traditional Methods</i> | | | | | | |
| R2Gen | 0.6004 | 0.4703 | 0.3807 | 0.3138 | 0.3605 | 0.0232 |
| R2GenCMN | 0.6232 | 0.5178 | 0.4420 | 0.3838 | 0.7065 | 0.0650 |
| R2GPT | 0.7324 | 0.6446 | 0.5777 | 0.5231 | 0.8389 | <u>0.2589</u> |
| CvT2DistilGPT2 | 0.6249 | 0.5224 | 0.4485 | 0.3904 | 0.4131 | 0.0268 |
| R2GenCSR | 0.7216 | 0.6372 | 0.5710 | 0.5165 | 0.8386 | 0.1786 |
| <i>MLLM</i> | | | | | | |
| MedGemma | 0.6489 | 0.5562 | 0.4867 | 0.4318 | 0.7921 | 0.0986 |
| LLaVA-Med | 0.7242 | 0.6266 | 0.5521 | 0.4935 | 0.8345 | 0.1741 |
| Qwen2.5-VL | 0.6873 | 0.5853 | 0.5098 | 0.4506 | 0.7947 | 0.1382 |
| <i>Fact-Flow</i> | | | | | | |
| MedGemma + FF | 0.7079 | 0.6267 | 0.5627 | 0.5099 | 0.8272 | 0.2306 |
| LLaVA-Med + FF | 0.7685 | <u>0.6798</u> | <u>0.6103</u> | <u>0.5533</u> | <u>0.8457</u> | 0.2350 |
| Qwen2.5-VL + FF | <u>0.7681</u> | 0.6820 | 0.6133 | 0.5567 | 0.8558 | 0.2759 |

guidance enables more precise localization of findings (e.g., disease laterality, anatomical region) compared to the vanilla MLLM baseline.

3.4 Analysis of Visual and Factual Guidance

We evaluate five configurations on the tuberculosis dataset using Qwen2.5-VL (Table 4), varying input modalities (image and/or label) and label sources (predicted vs. ground-truth). The **Image Only** baseline suffers from mode collapse despite high precision, as MLLMs generate overly conservative reports

Table 3. Case study of generated reports on the Tuberculosis dataset. Text with green background indicates correct findings matching ground truth, while red background indicates incorrect or missing findings.

| Chest X-ray | Ground Truth | MLC Prediction | MedGemma Fact-Flow | + | MedGemma |
|---|---|---|---|---|---------------|
|  | Right secondary PTB in the upper and middle fields | Pulmonary tuberculosis, Secondary (post-primary) pulmonary tuberculosis | secondary PTB in the right upper field | | bilateral PTB |
| RadFact F1 | | | 1 | | 0 |
|  | extensive infiltrates bilaterally with large cavity in RUL and a moderate pleural effusion on the left. AFB smears and RNA probes pos for MTB. Active TB, cavitory. | Pulmonary tuberculosis, Pulmonary cavitation, Pulmonary infiltrates, Pleural effusion | bilateral PTB with cavitation and left pleural effusion | | bilateral PTB |
| RadFact F1 | | | 0.67 | | 0 |

Table 4. Analysis of visual and factual guidance on the Tuberculosis dataset using Qwen2.5-VL. “Pred” and “GT” denote predicted and ground-truth labels, respectively.

| Input Modality | | Clinical Efficacy | | | Natural Language Generation | | | | | |
|---------------------------------|-------|-------------------|---------------|---------------|-----------------------------|---------------|---------------|---------------|---------------|---------------|
| Image | Label | F1 | Prec. | Recall | B-2 | B-3 | B-4 | R-L | CIDEr | METEOR |
| <i>Practical Configurations</i> | | | | | | | | | | |
| ✓ | - | 0.0286 | 1.0000 | 0.0145 | 0.0265 | 0.0265 | 0.0265 | 0.4779 | 1.2035 | 0.1141 |
| - | Pred | 0.2115 | 0.2656 | 0.1757 | 0.2895 | 0.2409 | 0.2074 | 0.5943 | 1.9209 | 0.2188 |
| ✓ | Pred | 0.2831 | 0.3535 | 0.2361 | 0.2951 | 0.2455 | 0.2129 | 0.6107 | 1.9434 | 0.2236 |
| <i>Oracle Upper Bounds</i> | | | | | | | | | | |
| - | GT | 0.3750 | 0.5000 | 0.3000 | 0.3658 | 0.3026 | 0.2618 | 0.6990 | 2.3198 | 0.2691 |
| ✓ | GT | 0.4421 | 0.5116 | 0.3892 | 0.3727 | 0.3095 | 0.2680 | 0.7198 | 2.4420 | 0.2746 |

without factual grounding. Introducing predicted labels (**Label Only (Pred)**) substantially improves both clinical efficacy and NLG metrics, and combining image with predicted labels (**Image + Label (Pred)**)—our full Fact-Flow approach—achieves the best practical performance, confirming that visual context and factual guidance are complementary. The performance gap between predicted and ground-truth label conditions highlights label quality as the key bottleneck, and the oracle **Image + Label (GT)** consistently outperforms **Label Only (GT)**, indicating that visual information provides spatial details that discrete labels alone cannot capture.

3.5 Intermediate Stage Analysis

We validate each intermediate pipeline stage (Table 5). **Stage 1:** All metrics are verified by a professional ophthalmologist on the ophthalmology dataset.

Table 5. Intermediate stage analysis. **Left:** Intrinsic quality evaluation of Stage 1 on the ophthalmology dataset (all metrics verified by a professional ophthalmologist). Report-level metrics (Coverage, LLM-Match Accuracy) are measured on 50 randomly sampled reports; label-level metrics (Redundancy, Clinical Validity) characterize \mathcal{L} itself. **Right:** Stage 2 MLC classification performance on test sets.

| Stage 1 | Result | Stage 2 | Macro-F1 | Micro-F1 |
|---|--------------|---------------|----------|----------|
| <i>Report-level (50 sampled reports)</i> | | | | |
| Coverage | 100% (50/50) | | | |
| LLM-Match Accuracy | 100% (50/50) | | | |
| <i>Label-level (\mathcal{L})</i> | | | | |
| Redundancy | 7.5% | Tuberculosis | 0.5227 | 0.7328 |
| Valid & decidable | 80% | Ophthalmology | 0.7071 | 0.8426 |
| Valid, context-dependent | 15% | | | |
| Overly generic | 5% | | | |
| Invalid / pseudo-concept | 0% | | | |

(1) **Coverage** measures whether each report’s key clinical information can be expressed by a subset of labels in \mathcal{L} , rated as *fully / partially / not covered* on 50 randomly sampled reports; (2) **LLM-Match Accuracy** checks whether LLM-Match assigns correct labels (set-level) on the same 50 reports; (3) **Redundancy** estimates the proportion of clinically synonymous label pairs within \mathcal{L} ; and (4) **Clinical Validity** categorizes each label as *valid & decidable*, *valid but context-dependent*, *overly generic*, or *invalid/pseudo-concept*. Results confirm 100% coverage and matching accuracy, low redundancy (7.5%), and 80% of labels valid and decidable with none invalid, validating the bootstrapped vocabulary. **Stage 2:** The MLC achieves Macro-/Micro-F1 of 0.52/0.73 on tuberculosis and 0.71/0.84 on ophthalmology, providing sufficient grounding for Stage 3.

4 Conclusion

To address the critical challenge of factual instability in Multimodal Large Language Models (MLLMs) when applied to medical report generation, we propose Fact-Flow, a novel framework that enhances factual accuracy by decoupling visual feature recognition from textual composition. Our core contributions include an LLM-bootstrapped pipeline for automatic multi-label dataset creation and a multi-label classification model that provides an explicit “Fact-Flow” to guide the MLLM. Fact-Flow is a plug-and-play framework compatible with any MLLM architecture, particularly suited to clinical scenarios where reports revolve around targeted and enumerable finding categories. Experiments on two disease-focused datasets with three MLLMs (Qwen2.5-VL, MedGemma, and LLaVA-Med) demonstrate that Fact-Flow consistently and significantly improves the factual correctness of generated reports over state-of-the-art methods and direct fine-tuning, without compromising textual quality.

References

1. Bai, S., Chen, K., Liu, X., Wang, J., Ge, W., Song, S., Dang, K., Wang, P., Wang, S., Tang, J., et al.: Qwen2. 5-vl technical report. arXiv preprint arXiv:2502.13923 (2025)
2. Banerjee, S., Lavie, A.: Meteor: An automatic metric for mt evaluation with improved correlation with human judgments. In: Proceedings of the acl workshop on intrinsic and extrinsic evaluation measures for machine translation and/or summarization. pp. 65–72 (2005)
3. Bannur, S., Bouzid, K., Castro, D.C., Schwaighofer, A., Thieme, A., Bond-Taylor, S., Ilse, M., Pérez-García, F., Salvatelli, V., Sharma, H., et al.: Maira-2: Grounded radiology report generation. arXiv preprint arXiv:2406.04449 (2024)
4. Chen, Z., Shen, Y., Song, Y., Wan, X.: Cross-modal memory networks for radiology report generation. In: Proceedings of the 59th annual meeting of the association for computational linguistics and the 11th international joint conference on natural language processing (volume 1: long papers). pp. 5904–5914 (2021)
5. Chen, Z., Song, Y., Chang, T.H., Wan, X.: Generating radiology reports via memory-driven transformer. arXiv preprint arXiv:2010.16056 (2020)
6. Hu, E.J., Shen, Y., Wallis, P., Allen-Zhu, Z., Li, Y., Wang, S., Wang, L., Chen, W.: Lora: Low-rank adaptation of large language models. In: International Conference on Learning Representations (2022)
7. Jaeger, S., Candemir, S., Antani, S., Wang, Y.X.J., Lu, P.X., Thoma, G.: Two public chest x-ray datasets for computer-aided screening of pulmonary diseases. *Quantitative imaging in medicine and surgery* **4**(6), 475 (2014)
8. Jing, B., Xie, P., Xing, E.: On the automatic generation of medical imaging reports. In: Proceedings of the 56th annual meeting of the association for computational linguistics (volume 1: long papers). pp. 2577–2586 (2018)
9. Li, C.Y., Liang, X., Hu, Z., Xing, E.P.: Knowledge-driven encode, retrieve, paraphrase for medical image report generation. In: Proceedings of the AAAI conference on artificial intelligence. vol. 33, pp. 6666–6673 (2019)
10. Li, C., Wong, C., Zhang, S., Usuyama, N., Liu, H., Yang, J., Naumann, T., Poon, H., Gao, J.: Llava-med: Training a large language-and-vision assistant for biomedicine in one day. *Advances in Neural Information Processing Systems* **36**, 28541–28564 (2023)
11. Lin, C.Y.: Rouge: A package for automatic evaluation of summaries. In: Text summarization branches out. pp. 74–81 (2004)
12. Liu, F., Wu, X., Ge, S., Fan, W., Zou, Y.: Exploring and distilling posterior and prior knowledge for radiology report generation. In: Proceedings of the IEEE/CVF conference on computer vision and pattern recognition. pp. 13753–13762 (2021)
13. Liu, H., Li, C., Wu, Q., Lee, Y.J.: Visual instruction tuning. *Advances in neural information processing systems* **36**, 34892–34916 (2023)
14. Liu, Z., Mao, H., Wu, C.Y., Feichtenhofer, C., Darrell, T., Xie, S.: A convnet for the 2020s. In: Proceedings of the IEEE/CVF conference on computer vision and pattern recognition. pp. 11976–11986 (2022)
15. Menon, A.K., Jayasumana, S., Rawat, A.S., Jain, H., Veit, A., Kumar, S.: Long-tail learning via logit adjustment. arXiv preprint arXiv:2007.07314 (2020)
16. Miura, Y., Zhang, Y., Tsai, E., Langlotz, C., Jurafsky, D.: Improving factual completeness and consistency of image-to-text radiology report generation. In: Proceedings of the 2021 Conference of the North American Chapter of the Association for Computational Linguistics: Human Language Technologies. pp. 5288–5304 (2021)

17. Nicolson, A., Dowling, J., Koopman, B.: Improving chest x-ray report generation by leveraging warm starting. *Artificial intelligence in medicine* **144**, 102633 (2023)
18. Nooralahzadeh, F., Gonzalez, N.P., Frauenfelder, T., Fujimoto, K., Krauthammer, M.: Progressive transformer-based generation of radiology reports. arXiv preprint arXiv:2102.09777 (2021)
19. Papineni, K., Roukos, S., Ward, T., Zhu, W.J.: Bleu: a method for automatic evaluation of machine translation. In: *Proceedings of the 40th annual meeting of the Association for Computational Linguistics*. pp. 311–318 (2002)
20. Sellergren, A., Kazemzadeh, S., Jaroensri, T., Kiraly, A., Traverse, M., Kohlberger, T., Xu, S., Jamil, F., Hughes, C., Lau, C., et al.: Medgemma technical report. arXiv preprint arXiv:2507.05201 (2025)
21. Siméoni, O., Vo, H.V., Seitzer, M., Baldassarre, F., Oquab, M., Jose, C., Khalidov, V., Szafraniec, M., Yi, S., Ramamonjisoa, M., et al.: Dinov3. arXiv preprint arXiv:2508.10104 (2025)
22. Vedantam, R., Lawrence Zitnick, C., Parikh, D.: Cider: Consensus-based image description evaluation. In: *Proceedings of the IEEE conference on computer vision and pattern recognition*. pp. 4566–4575 (2015)
23. Wang, S., Tang, L., Lin, M., Shih, G., Ding, Y., Peng, Y.: Prior knowledge enhances radiology report generation. *AMIA Summits on Translational Science Proceedings* **2022**, 486 (2022)
24. Wang, X., Li, Y., Wang, F., Wang, S., Li, C., Jiang, B.: R2gensr: Retrieving context samples for large language model based x-ray medical report generation. arXiv preprint arXiv:2408.09743 (2024)
25. Wang, X., Peng, Y., Lu, L., Lu, Z., Summers, R.M.: Tienet: Text-image embedding network for common thorax disease classification and reporting in chest x-rays. In: *Proceedings of the IEEE conference on computer vision and pattern recognition*. pp. 9049–9058 (2018)
26. Wang, Z., Liu, L., Wang, L., Zhou, L.: R2gengpt: Radiology report generation with frozen llms. *Meta-Radiology* **1**(3), 100033 (2023)
27. Xue, Y., Xu, T., Rodney Long, L., Xue, Z., Antani, S., Thoma, G.R., Huang, X.: Multimodal recurrent model with attention for automated radiology report generation. In: *International Conference on Medical Image Computing and Computer-Assisted Intervention*. pp. 457–466. Springer (2018)